PFC/JA-94-05

X-ray Observations of Helium-like Scandium from the Alcator C-Mod Tokamak

J.E. Rice, M.A. Graf, J.L. Terry,
E.S. Marmar, K. Giesing, F. Bombarda[†]

Plasma Fusion Center
Massachusetts Institute of Technology
Cambridge, MA 02139

March, 1994

[†]Associazione ENEA-Euratom per la Fusion, Frascati, Italy.

Submitted to Physical Review A.

This work was supported by the U. S. Department of Energy Contract No. DE-AC02-78ET51013. Reproduction, translation, publication, use and disposal, in whole or in part by or for the United States government is permitted.

X-ray Observations of Helium-like Scandium from the Alcator C-Mod Tokamak

J.E.Rice, M.A.Graf, J.L.Terry, E.S.Marmar and K.Giesing

Plasma Fusion Center, M.I.T.
175 Albany St.
Cambridge, MA, 02139

F.Bombarda

Associazione ENEA-Euratom per la Fusione
C.P. 65, 00044
Frascati, Italy

Abstract

Scandium (Z=21) has been injected into the Alcator C-Mod tokamak. X-ray wavelengths of Δn=1 ground state transitions in Sc^{19+} and Sc^{18+} have been accurately determined. Spectra have been obtained from different radial locations and have been compared to the results of collisional-radiative-transport code modelling. The density of scandium in the plasma has been determined for a variety of operating conditions.

Introduction

Scandium has been injected into the Alcator C-Mod tokamak[1] using the laser blow-off technique[2], in order to study impurity transport[3-7]. A typical deuterium discharge into which scandium was injected is depicted in Fig. 1. Plasma parameters at the injection time of .550 s were B_T = 5.2 T, I_P = 1.0 MA, elongation = 1.6, T_{e0} = 1600 eV , n_{e0} = 1.6 x 10^{20} m^{-3} and the minor radius on the midplane = 22.5 cm. The nominal major radius (magnetic axis) of the plasma was 69.0 cm. Effects of the injection can be seen on the total radiated power, the central soft x-ray trace and Z_{eff}. Two of the diagnostics used to observe the injected scandium were an x-ray pulse height analysis system and a 5 chord, independently scannable high energy resolution crystal x-ray spectrometer array [8]. A spectrum of the scandium x-ray emission, taken from one of the crystal spectrometers viewing near the plasma center, is shown in Fig. 2. The spectrum is dominated by the resonance line (w). The intercombination (x,y) and forbidden (z) lines, as well as some satellites, are also visible.

Wavelength Determination

In order to identify all of the transitions in this spectrum, and to determine accurately the wavelengths, advantage has been taken of the occurance of several high n transitions of hydrogen-like argon in this same spectral range. In particular the 5p-, 6p-, 7p- and 8p-1s lines with precisely known wavelengths of 2917.50 mÅ, 2881.04 mÅ, 2859.38 mÅ and 2845.51 mÅ, respectively[9], have been used to calibrate the dispersion of the spectrometer [10]. Argon was puffed into the early phase of the discharge using a piezo-electric valve; a spectrum of these Ar^{17+} lines is shown in Fig. 3. For scandium, line identifications, relative intensities and measured wavelengths, along with calculated wavelengths[11-14] are given in Table 1. The measured wavelengths are accurate to ±.1 mÅ. The wavelengths from Ref.(14) are in excellent agreement for the helium-like lines, but there is a systematic shift

of about .8 mÅ for all of the transitions of Refs.(11-13), because QED effects were not taken into account.

Synthetic Spectra

A collisional-radiative model for the emissivities of helium-like ions[15,16] has been used in conjuction with the impurity transport code MIST[17] in order to calculate the chord brightness profiles of the lines in the Sc^{19+} spectrum. The n=2 levels in helium-like scandium are populated by collisional excitation of the helium-like state, inner shell ionization of the lithium-like state, and radiative and dielectronic recombination of the hydrogen-like state. Appropriate coefficients have been interpolated from the tables of Ref.(15). For the n = 2 and 3 dielectronic satellites, the values of the intensity factor 'q' have been taken from Refs.(11 and 12). For the inner shell satellites, excitation rates have been interpolated from the rates for lithium-like calcium[18] and titanium.[19] This allows for calculation of the emissivity profiles of all of the lines in the spectrum, given charge state density profiles and measured electron density and temperature profiles. The charge state density profiles are taken from MIST calculations, where the impurity transport is modelled typically with a spatially constant diffusion coefficient and with no convective velocity (v=0). Electron temperature and density profiles for the discharge of Fig. 1 are shown in Fig. 4, which were taken from ECE and laser interferometer measurements, respectively.

Emissivity profiles of all the lines have been calculated for a case with the plasma parameters of the shot shown in Fig. 1, and with a diffusion coefficient of 5000 cm^2/sec, consistent with a 1/e decay time of 19 ms for central brightness time histories. The emissivities (and charge state densities) are taken to be constant along each flux surface (reconstructed from the EFIT[20] code), and brightnesses corresponding to the actual spectrometer lines of sight are then calculated. From these brightnesses, synthetic spectra are then constructed, with the wavelengths of

the helium-like lines taken from Ref.(14), and with the satellites of Refs.(11 and 12) shifted by .8 mÅ towards the red. Appropriate line widths from measured ion temperatures and instrumental widths are also employed. An example is shown in Fig. 5, for a total of 5 x 10^{17} injected scandium atoms, to be compared with the spectrum of Fig. 2. In this case the brightnesses were integrated over the entire time the scandium was in the plasma. The satellites with n>3 spectators, and those with wavelengths longer than 2905 mÅ have not been included. The agreement between the synthetic and observed spectrum is good, supportive of the collisional-radiative model, the transport coefficients and the observed electron temperature profile.

Spatial and Temporal Variations

Since there are 5 spectrometers viewing along different chords in the plasma, spatial information about the Sc^{19+} brightness profiles is available for these injections. Shown in Fig. 6 are the 5 spectrometer lines of sight superimposed on the flux surface recontructions for a particular discharge. The origin of the coordinate system used to describe the spectrometer views is the nominal center of the machine, located at Z = 0 and R = 67.0 cm, and is indicated by an 'X'. The magnetic axis of this discharge at the time of the injection (.8 sec) was at Z = -2.3 cm and R = 69.3 cm, and is indicated by a '+' symbol. In the lower right corner are listed the vertical locations (in meters) where the 5 lines of sight intersect the vertical plane at R = 67.0 cm. Just to the left of these numbers are listed the radii of the innermost flux surfaces (mapped onto the magnetic horizontal midplane on the outer half of the plasma) that the spectrometer lines of sight intersect (are tangent to). These locations are indicated on the magnetic midplane by a different symbol for each spectrometer. For example, the spectrometer 5 line of sight intersects the vacuum vessel center vertical plane (R = 67.0 cm) at 16.0 cm above the center (Z = +16.0 cm). The innermost flux surface that this line of sight intersects can be traced back to R = 83.0 cm on the magnetic midplane (Z = -2.3 cm), which is indicated by a

square.

Shown in Fig. 7 by the narrow line is a spectrum taken along a line of sight which crosses the R = 67.0 cm vertical plane 12.7 cm below the midplane (R = 77.3 cm), for a discharge similar to that shown in Fig. 1. The highest electron temperature along this chord for this discharge was around 1200 eV. Notice that the intensities of the intercombination and forbidden lines, as well as the satellites, have grown relative to the resonance line. Shown in Fig. 7 by the heavy line is a synthetic spectrum calculated for the line of sight of the observed spectrum. Again, the agreement between the observed and calculated spectra is quite good. In fact this situation persists out at least to 80% of the minor radius. Shown in Fig. 8 by the narrow line is a spectrum taken from along a line of sight 18.3 cm above the midplane (R = 83.8 cm), where the maximum electron temperature was around 600 eV. Although the signal level is very low, it is clear that the forbidden line intensity is greater than or equal to that of the resonance line, indicative of a recombining plasma.[21] Also in Fig. 8 is shown the corresponding synthetic spectrum (heavy line), again with fairly good qualitative agreement.

In Fig. 9 are shown the ratios of the forbidden line z, the inner shell satellite q and the dielectronic satellite k to the resonance line w taken along 4 lines of sight. The horizontal axis is the major radius on the plasma midplane of the inner-most flux surface to which the individual line of sight is tangent. These lines, as well as in fact all lines in the spectrum, increase relative to the resonance line with increasing distance away from the plasma center, at least out to 84 cm (r/a = .8). The curves are the ratios from the calculated brightness profiles.

All of the results discussed above are based on spectra integrated over the duration of the injections. Temporal information is also available from the spectrometer array. Shown in Fig. 10 are the time histories of three total spectrometer signals, integrated over the wavelength region between 2.86 and 2.94 Å as functions of time. In this case the injection time was .550 sec. The three traces were from spectrometers looking at +3.0, -12.7 and +18.3 cm, respectively. The signals all

decay with a 1/e time about 19 ms, which implies a diffusion coefficient of about 5000 cm^2/sec. Notice that the signal at -12.7 cm (b.) rises to a peak in about 5 ms, nearly a factor of 2 faster than the more central chord (a.). However, the outermost signal at 18.3 cm (c.) actually peaks later than that of the central chord. This is because, at these extreme radii, the upper levels for the lines are mainly populated by radiative recombination of hydrogen-like Sc^{20+} and during the influx phase of the injection, there is no hydrogen-like scandium at this radius. Also shown (by the smooth curves) are the code results, which are in excellent agreement.

There is also spectral information available as a function of time. For all of these injections, spectra were collected with 50 ms integration time during the discharges, and although these injections were relatively fast (a typical total duration was 80 ms), at least 2 spectra were collected per injection. For the spectrometer looking at -9.4 cm (R = 74.2 cm), differences were seen in the first 25 ms 'ionization' phase of the injections and the last 50 ms 'decay' phase. In particular, the inner shell satellites were all stronger relative to the resonance line during the rise phase. The upper levels of these inner shell satellites are mainly populated by excitation of lithium-like Sc^{18+}. Shown in Fig. 11 are the ratios of several satellites to the resonance line during the rise phase (left edges of the lines) and the decay phase (right edges). The satellites q and r are brighter during the early phase due to a greater abundance of Sc^{18+} at this time. This point is supported by the code modelling.

In order to emphasize this, and to explain quantitatively the later peaking of the total line brightness time history at the outermost chord, brightness time histories of the individual lines have been calculated. Time histories for q, w and z for the line of sight 18.3 cm above the midplane (R = 83.8 cm) are shown in Fig. 12. Each line demonstrates the dominance of a different charge state in the population of the upper level, for q the lithium-like stage, for w helium-like, and for z hydrogen-like. These three charge states appear at this radius sequentially in time, the Li-like as the scandium diffuses into the center and the H-like as the scandium leaves the

plasma. This is corroborated in Fig. 13 which shows the calculated charge state density profiles for lithium-like (18+), helium-like (19+) and hydrogen-like (20+) scandium at three different times after the injection. Shown by the dotted lines are the profiles at 1.7 ms, by the solid lines the profiles at 4.2 ms and by the dashed lines the profiles at 25 ms. At R = 84 cm, the lithium-like state has the highest density at 1.7 ms. At 4.2 ms at this radius, the helium-like state dominates. At the latest time shown, 25 ms, the hydrogen-like scandium density is it's highest relative to the helium-like density. Since radiative recombination overwhelmingly dominates the population of the triplet levels of Sc^{19+} at the electron temperature of this radius, this amount of Sc^{20+} allows the forbidden line, z, to dominate the spectrum.[21] Synthetic spectra at three different times for this view (R = 83.8 cm) are shown in Fig. 14. In Fig. 14a, from 0-3.4 ms (the ionizing phase of the injection), the inner shell satellites are the strongest lines in the spectrum. From 3.6-6.6 ms (Fig. 14b), the resonance line is strongest and in Fig. 14c, from 11.6-48.5 ms, the forbidden line is dominant (the recombining phase).

Scandium Density Estimates

The absolute sensitivities of the spectrometers have been calculated from geometric factors, crystal reflectivities, window transmissions and detector sensitivities. (Impurity densities for argon, for example, determined from line brightnesses are in agreement with densities determined by two independent methods, namely from the x-ray PHA and from rises in Z_{eff} during argon puffing.) From scandium line brightnesses, the scandium density during an injection can be determined from knowledge of the electron density and temperature profiles, line population modelling and charge state profiles. For the discharge of Fig. 1, the deduced central scandium density at the peak of the injection was 6 x 10^{10} cm^{-3}, yielding a contribution to Z_{eff} of 0.13. This is consistent with a measured rise in Z_{eff} from visible bremsstrahlung of 0.12. Typically, 5 x 10^{17} atoms are injected at the edge, implying, for a plasma volume of .92 m^3, that at least 10% of the scandium is reaching the

plasma core. This is a considerably larger percentage of penetration than observed for argon introduced at room temperature through a gas valve.

Similar amounts of scandium were injected into a variety of plasma conditions. Shown in Fig. 15 is the deduced scandium density as a function of central electron density for a series of 850 kA plasmas. At the higher electron densities, less scandium is actually reaching the center, indicating a possible screening effect due to changes in the edge conditions. In discharges with higher central electron densities, the edge electron densities were also higher. The measured transport coefficients were unchanged during this density scan. Intrinsic impurity densities in the plasma are also lower at higher electron densities.

Conclusions

Scandium has been injected into Alcator C-Mod plasmas. Accurate x-ray wavelengths of $\Delta n = 1$ ground state transitions in Sc^{19+} and Sc^{18+} have been determined. Spectra have been obtained from various locations in the plasma and upper levels are populated by excitation and dielectronic recombination over most of the plasma volume and by radiative recombination in the edge regions. Observed spectra and brightness time histories are in good agreement with synthetic spectra and time histories calculated from a model which includes anomalous impurity transport, observed electron density and temperature profiles and collisional-radiative line emissivities. Absolute scandium densities have been determined for a variety of conditions. In a typical case, about 10% of the injected scandium penetrates the plasma edge to reach the center and there is an indication that less injected scandium penetrates to the core as the electron density is increased.

Acknowledgements

The authors would like to thank Amanda Hubbard for electron temperature

measurements, Tom Luke for electron density measurements, Steve Wolfe for flux surface reconstructions and Ying Wang for assistance with the spectrometers. Work supported by U.S. DoE Contract No. DE-AC02-78ET51013

References

[1] I. H. Hutchinson et al., Physics of Plasmas, in press

[2] E. Marmar, J. Cecchi and S. Cohen, Rev. Sci. Instrum. **46**, 1149 (1975)

[3] S. Suckewer et al., Phys. Lett. **80A**, 259 (1980)

[4] E. S. Marmar, J. E. Rice and S. L. Allen, Phys Rev. Lett. **45**, 2025 (1980)

[5] TFR Group, Phys. Lett. **87A**, 169 (1982)

[6] E. S. Marmar, J. E. Rice, J. L. Terry and F. Seguin, Nucl. Fusion **22**, 1567 (1982)

[7] M. Shimada, Fusion Engineering and Design **15**, 325 (1992)

[8] J. E. Rice and E. S. Marmar, Rev. Sci. Instrum. **61**, 2753 (1990)

[9] G. W. Erickson, J. Phys. Chem. Ref. Data **6**, 831 (1977)

[10] P. Beiersdorfer et al., Phys. Rev. A, **37**, 4153 (1988)

[11] L. A. Vainshtein and U. I. Safronova, Atomic Data and Nuclear Data Tables **21**, 49 (1978)

[12] L. A. Vainshtein and U. I. Safronova, Atomic Data and Nuclear Data Tables **25**, 311 (1980)

[13] V. A. Boiko et al., Mon. Not. R. Astr. Soc. **185**, 305 (1978)

[14] L. A. Vainshtein and U. I. Safronova, Physica Scripta **31**, 519 (1985)

[15] R. Mewe and J. Schrijver, Astron. Astrophys. **65**, 99 (1978)

[16] R. Mewe, J. Schrijver and J. Sylwester, Astron. Astrophys. **87**, 55 (1980)

[17] R. A. Hulse, Nucl. Tech./Fus. **3**, 259 (1983)

[18] F. Bely-Dubau et al., Mon. Not. R. Astr. Soc. **201**, 1155 (1982)

[19] F. Bely-Dubau et al., Phys. Rev. A **26**, 3459 (1982)

[20] L. L. Lao et al., Nucl. Fusion **25**, 1611 (1985)

[21] J. E. Rice, E. S. Marmar, E. Källne, and J. Källne, Phys. Rev. A **35**, 3033 (1987)

Table 1

Name	Transition	Rel. Int.	λ (mÅ)	$\lambda^{11,12,13}$	λ^{14}
w	$1s2p\ ^1P_1$ -$1s^2\ ^1S_0$	1.000	2873.1	2872.3	2873.2
4	1s2p4p-$1s^24p$	0.065	2875.0	-	-
3	$1s2p3p\ ^2D_{5/2}$ -$1s^23p\ ^2P_{3/2}$	0.064	2877.7	2876.2	-
x	$1s2p\ ^3P_2$ -$1s^2\ ^1S_0$	0.103	2883.2	2882.4	2883.3
s	$1s2s2p\ ^2P_{3/2}$ -$1s^22s\ ^2S_{1/2}$	0.056	2884.9	2883.8	-
y	$1s2p\ ^3P_1$ -$1s^2\ ^1S_0$	0.154	2887.0	2886.1	2887.0
q	$1s2s2p\ ^2P_{3/2}$ -$1s^22s\ ^2S_{1/2}$	0.049	2893.2	2892.4	-
r	$1s2s2p\ ^2P_{1/2}$ -$1s^22s\ ^2S_{1/2}$	0.032	2895.7	2895.2	-
k	$1s2p^2\ ^2D_{3/2}$ -$1s^22p\ ^2P_{1/2}$	0.043	2898.2	2897.4	-
j	$1s2p^2\ ^2D_{5/2}$ -$1s^22p\ ^2P_{3/2}$	0.030	2901.2	2901.0	-
z	$1s2p\ ^3S_1$ -$1s^2\ ^1S_0$	0.224	2902.8	2902.2	2903.0
β	$1s2s^22p\ ^1P_1$ -$1s^22s^2\ ^1S_0$	0.028	2911.5	2910.7	-
-	$1s2s2p\ ^4P_{3/2}$ -$1s^22s\ ^2S_{1/2}$	0.025	2915.7	2914.4	-
?	?	0.012	2919.3	-	-

The Δ n = 1 transitions of Sc^{19+} and Sc^{18+}. The measured wavelengths are given in the 4^{th} column. In the last column are the theoretical wavelengths of helium-like scandium from Vainshtein and Safronova[14]. In the penultimate column are theoretical wavelengths for helium-like scandium and the satellites with the spectator electron in the n = 2 level from Vainshtein and Safronova[11], an n = 3 spectator satellite from Vainshtein and Safronova[12] and a beryllium-like satellite from Boiko et al.[13]

Figure Captions

Fig. 1 The time histories of several parameters of interest for a discharge into which scandium was injected.

Fig. 2 The $\Delta n=1$ spectrum of helium-like Sc^{19+}.

Fig. 3 5p-, 6p-, 7p- and 8p-1s transitions in hydrogen-like Ar^{17+}.

Fig. 4 Electron temperature and density profiles for the discharge shown in Fig. 1.

Fig. 5 A synthetic spectrum of Sc^{19+} and satellites for plasma parameters similar to those for the observed spectrum of Fig. 2.

Fig. 6 Five spectrometer lines of sight superimposed on flux surface reconstructions.

Fig. 7 An observed scandium spectrum (thin line) from 12.7 cm below the midplane (R = 77.3 cm) and the corresponding synthetic spectrum (thick line).

Fig. 8 An observed scandium spectrum (thin line) from 18.3 cm above the midplane (R = 83.8 cm) and the corresponding synthetic spectrum (thick line).

Fig. 9 Observed (symbols) and calculated (curves) line ratios of z/w, q/w and k/w vs. major radius. Typical error bars are shown.

Fig. 10 Observed time histories of scandium injection along chords at a.) +3.0 cm, b.) -12.7 cm and c.) +18.3 cm, with code predictions (smooth lines). The injection time was at .550 sec.

Fig. 11 The ratios of the brightnesses at -9.4 cm of several satellites to the

resonance line at two different times during an injection, the first 25 ms and the last 50 ms.

Fig. 12 Calculated brightness time histories of q, w and z for a chord viewing 18.3 cm above the midplane (R = 83.8 cm.), as a function of time after the injection.

Fig. 13 Charge state density profiles for lithium-like (18+), helium-like (19+) and hydrogen-like (20+) scandium at three different times after the injection. Dotted lines - 1.7 ms, solid lines - 4.2 ms and dashed lines - 25 ms.

Fig. 14 Calculated spectra for a chord viewing 18.3 cm above the midplane (R = 83.8 cm) for three different times after the injection, a.) 0-3.4 ms, b.) 3.6-6.6 ms and c.) 11.6-48.5 ms.

Fig. 15 Scandium density scaling with central electron density. The curve is the best power law fit to the data, proportional to $n_{e0}{}^{-.78}$.

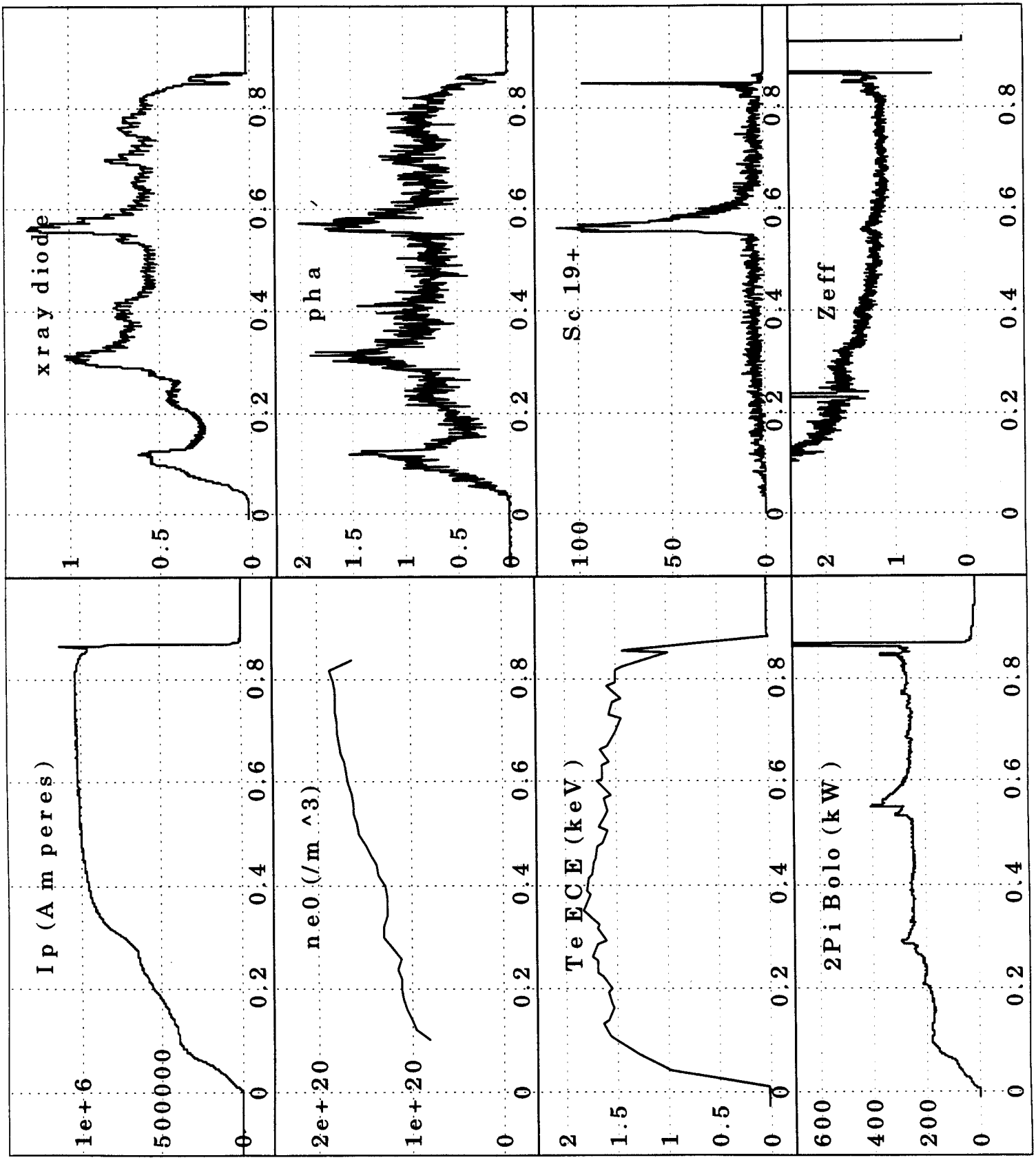
Ip (Amperes)
1e+6
500000
0
0
0.2
0.4
0.6
0.8
neO (/m^3)
2e+20
1e+20
0
0
0.2
0.4
0.6
0.8
Te ECE (keV)
2
1.5
1
0.5
0
0
0.2
0.4
0.6
0.8
2Pi Bolo (kW)
600
400
200
0
0
0.2
0.4
0.6
0.8
xray diode
1
0.5
0
0
0.2
0.4
0.6
0.8
pha
2
1.5
1
0.5
0
0
0.2
0.4
0.6
0.8
Sc 19+
100
50
0
0
0.2
0.4
0.6
0.8
Zeff
2
1
0
0
0.2
0.4
0.6
0.8

Figure 1

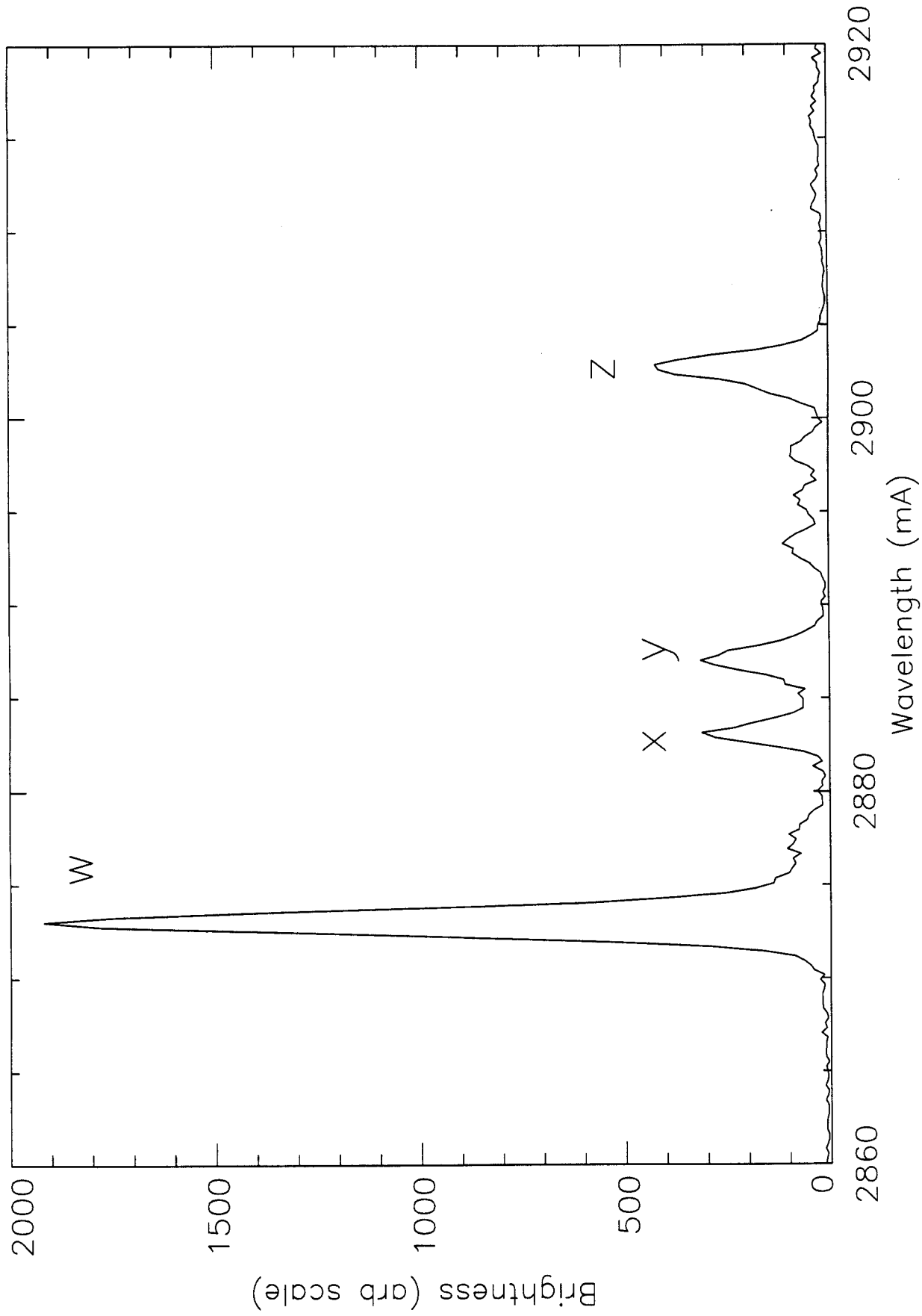
Brightness (arb scale)
2000
1500
1000
500
0
2860
2880
2900
2920
Wavelength (mA)
W
X
Y
Z

Figure 2

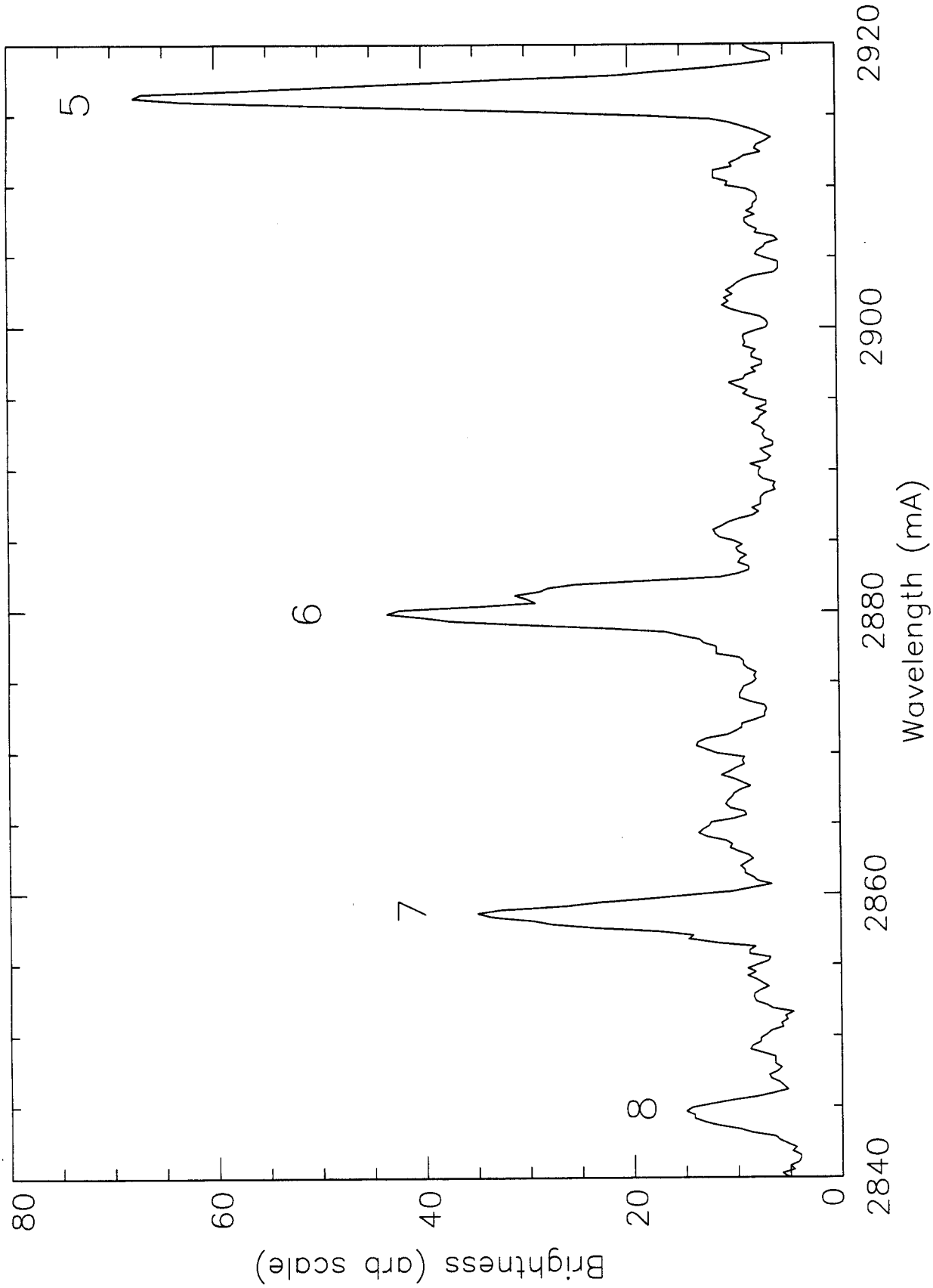
Brightness (arb scale)
0
20
40
60
80
2840
2860
2880
2900
2920
Wavelength (mA)
5
6
7
8

Figure 3

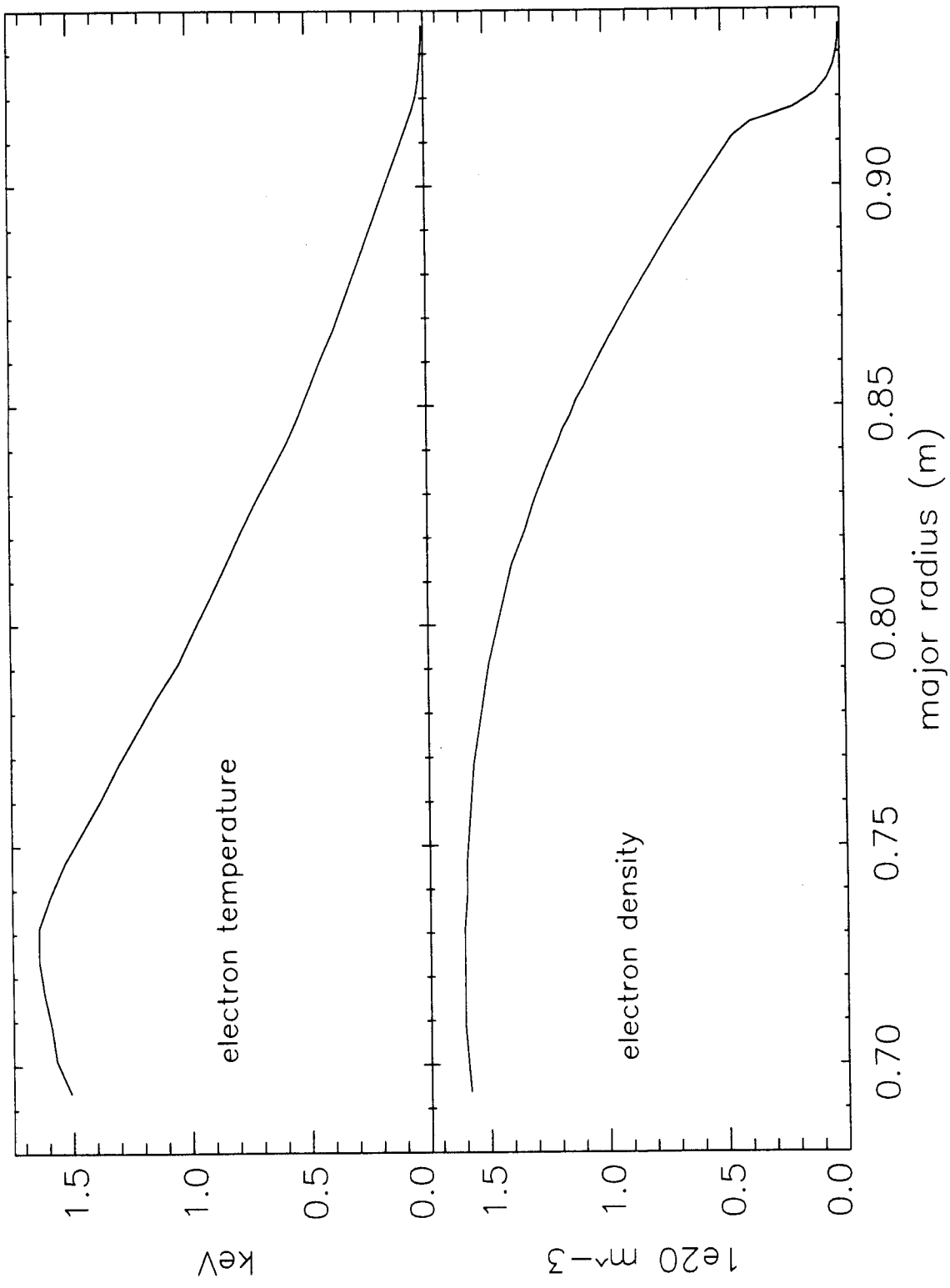
electron temperature
keV
1.5
1.0
0.5
0.0
electron density
1e20 m^-3
1.5
1.0
0.5
0.0
0.70
0.75
0.80
0.85
0.90
major radius (m)

Figure 4

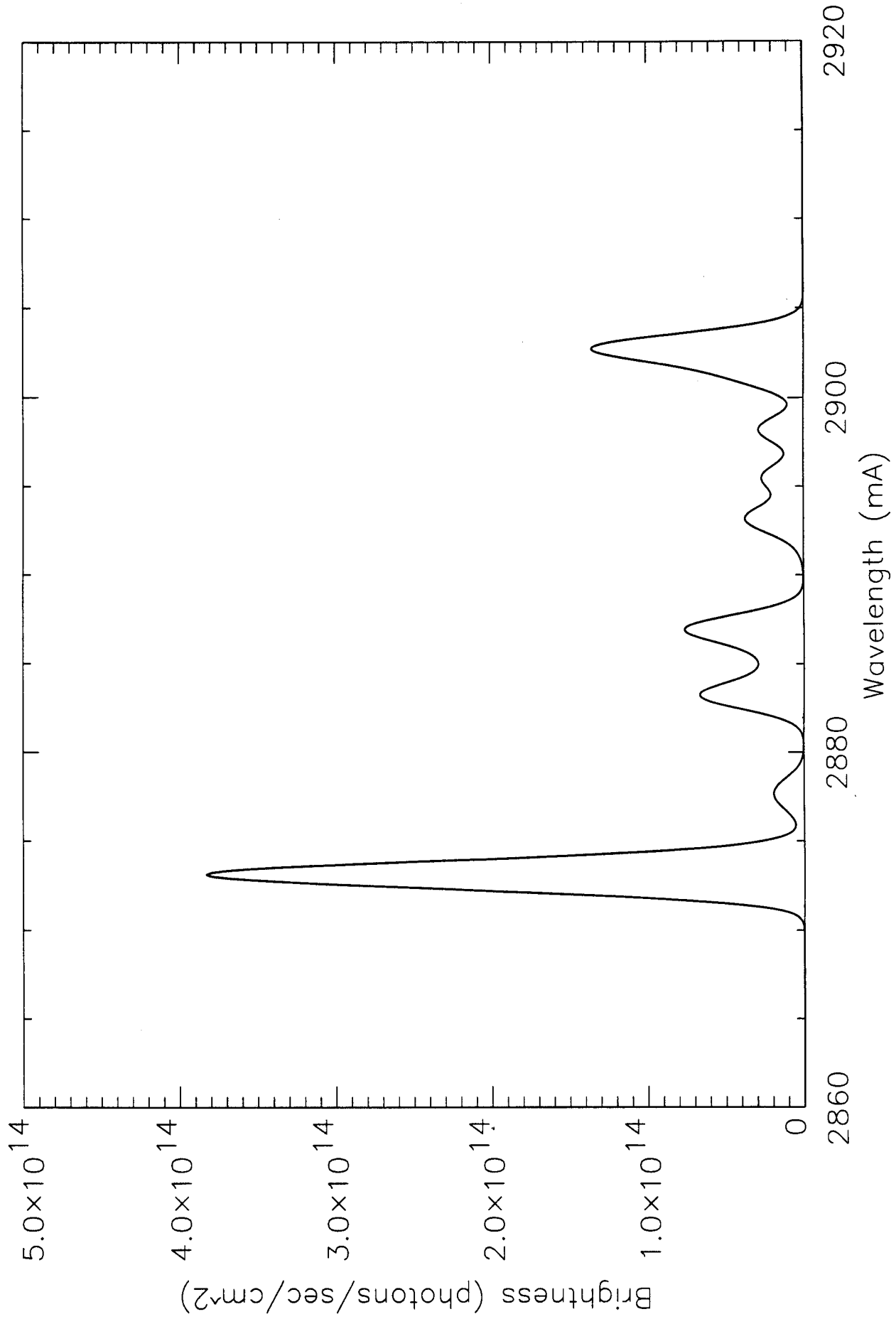
Brightness (photons/sec/cm^2)
5.0×10^14
4.0×10^14
3.0×10^14
2.0×10^14
1.0×10^14
0
2860
2880
2900
2920
Wavelength (mA)

Figure 5

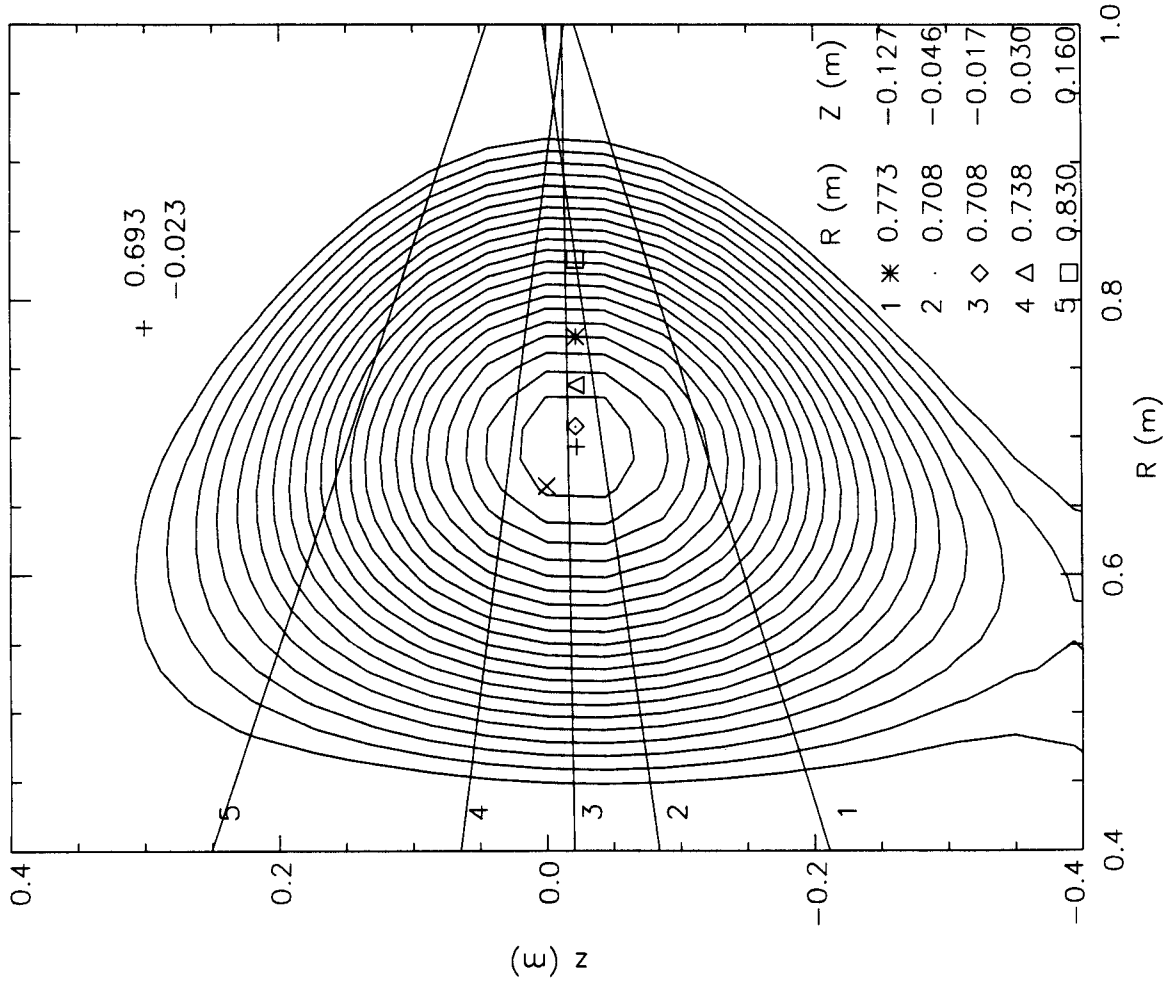
+ 0.693
−0.023
R (m) Z (m)
1 ✳ 0.773 −0.127
2 · 0.708 −0.046
3 ◇ 0.708 −0.017
4 △ 0.738 0.030
5 □ 0.830 0.160
0.4
0.2
0.0
−0.2
−0.4
z (m)
0.4
0.6
0.8
1.0
R (m)
1
2
3
4
5

Figure 6

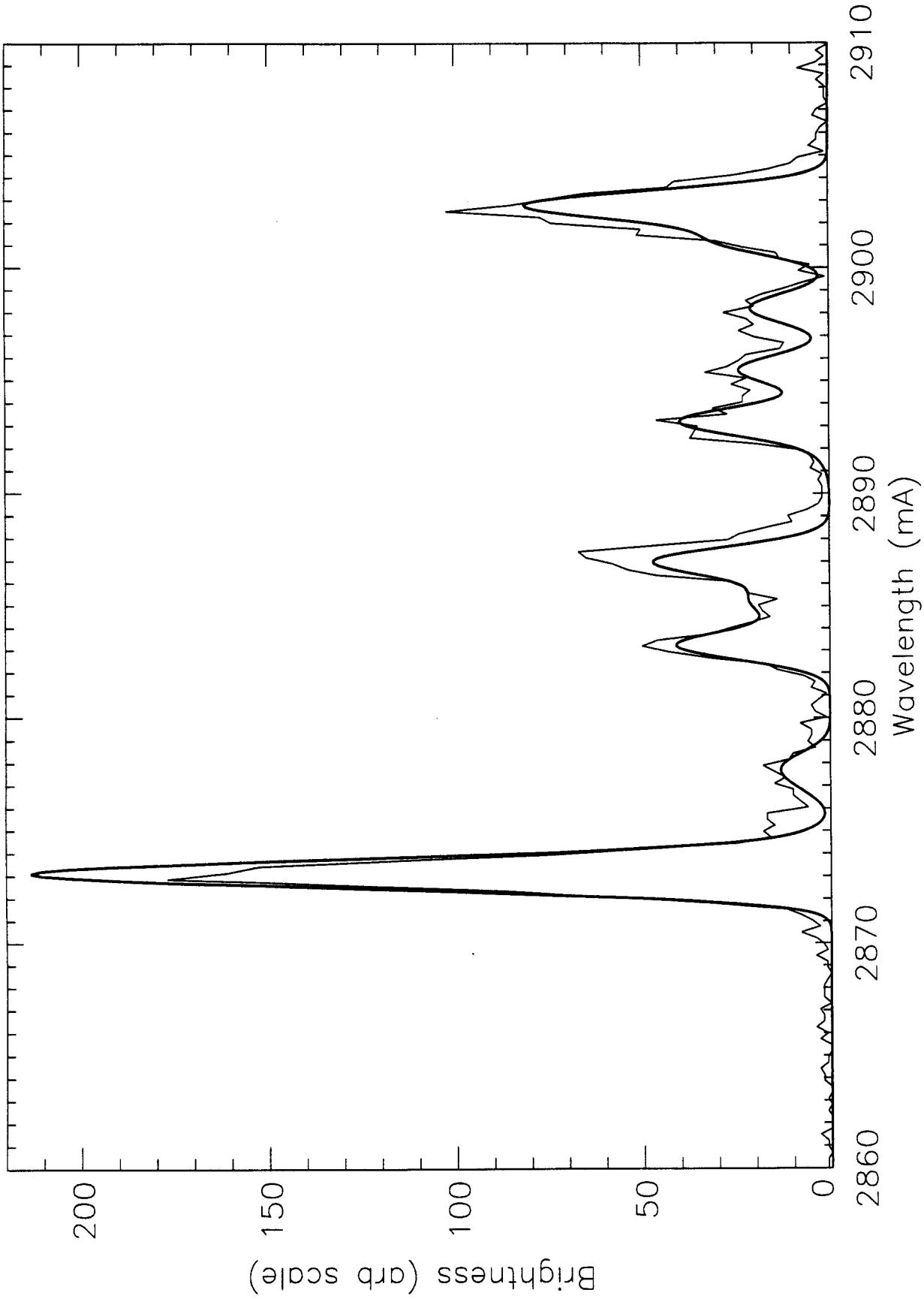
Brightness (arb scale)
0
50
100
150
200
2860
2870
2880
2890
2900
2910
Wavelength (mA)

Figure 7

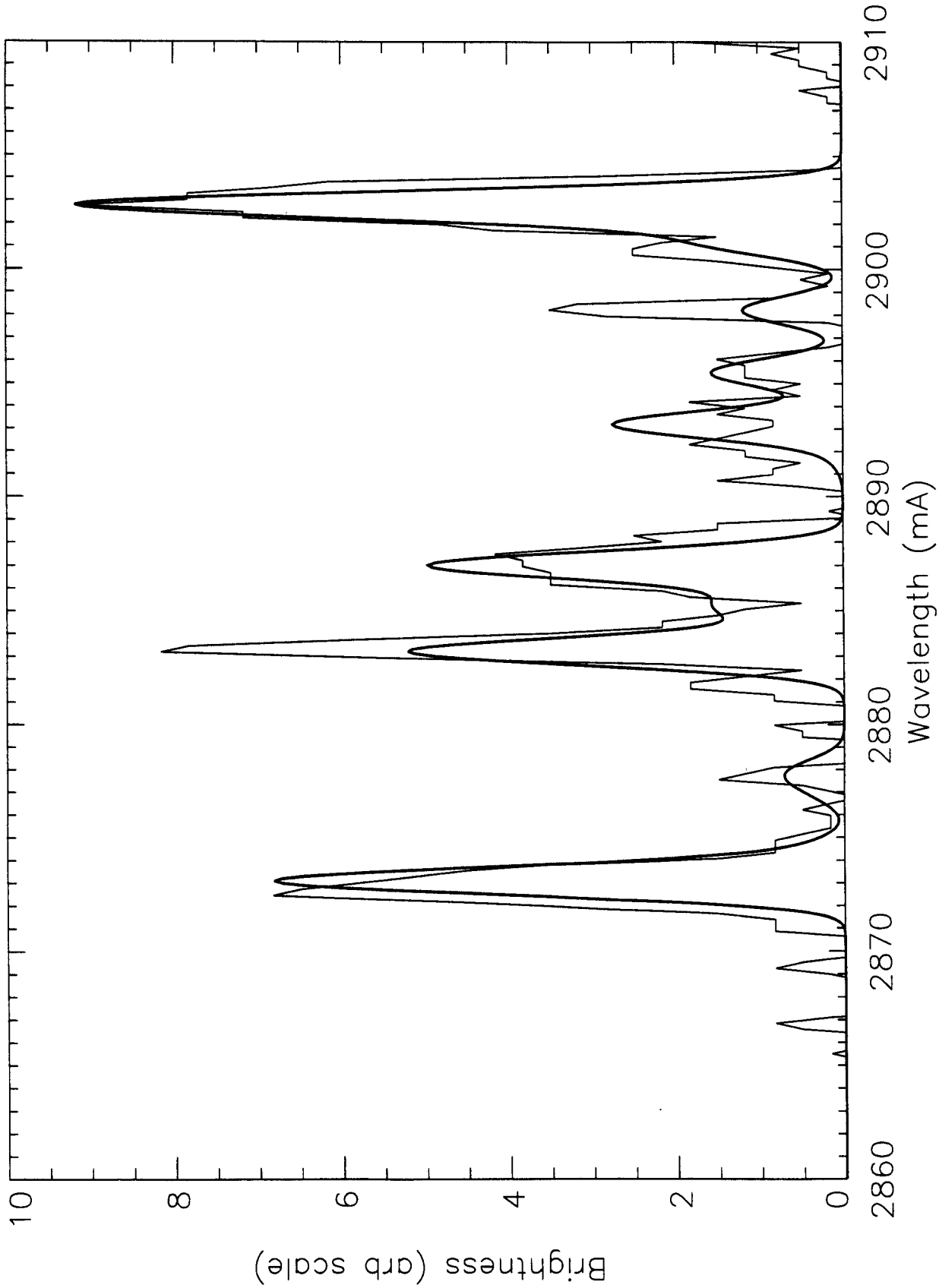
Brightness (arb scale)
0
2
4
6
8
10
2860
2870
2880
2890
2900
2910
Wavelength (mA)

Figure 8

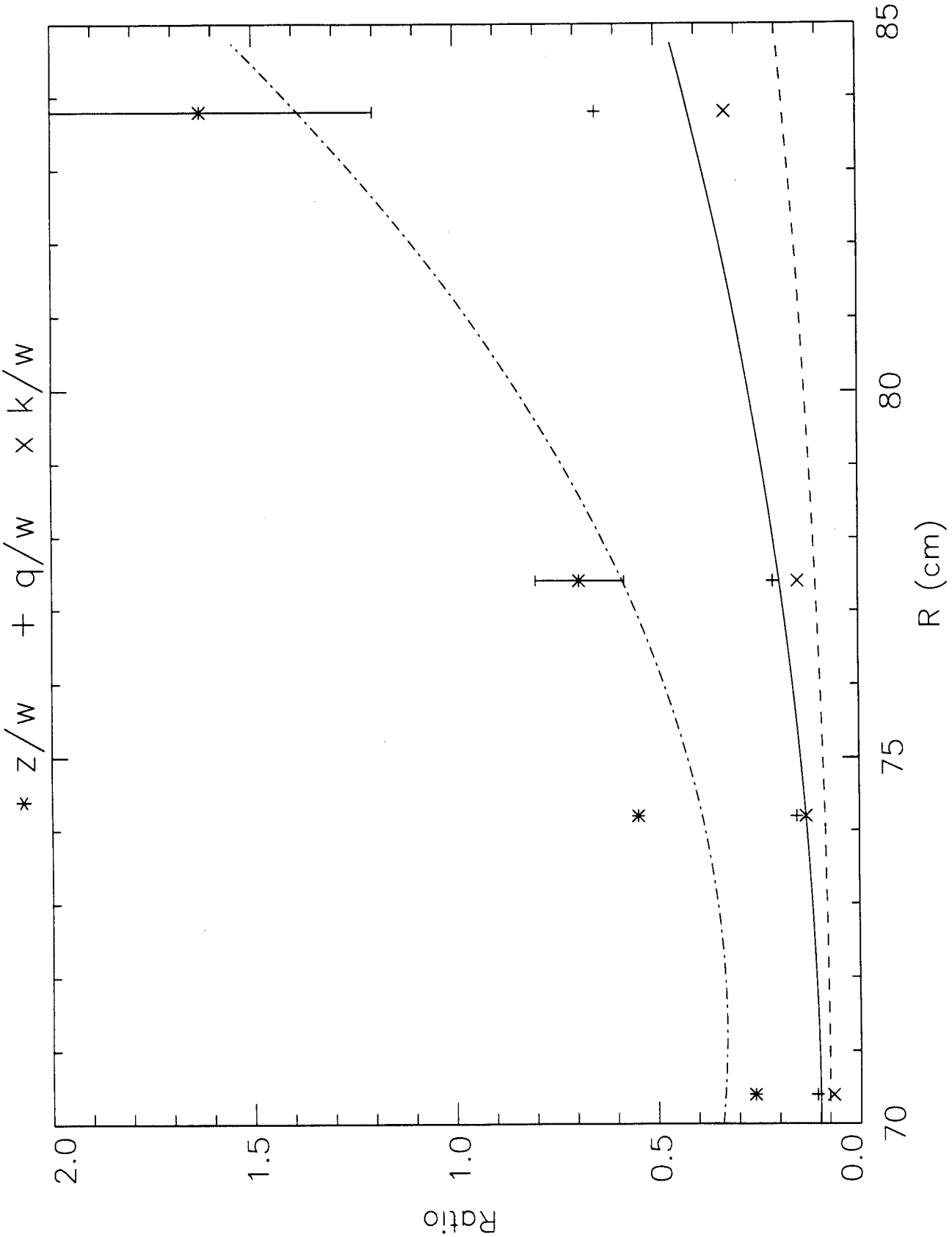

Figure 9

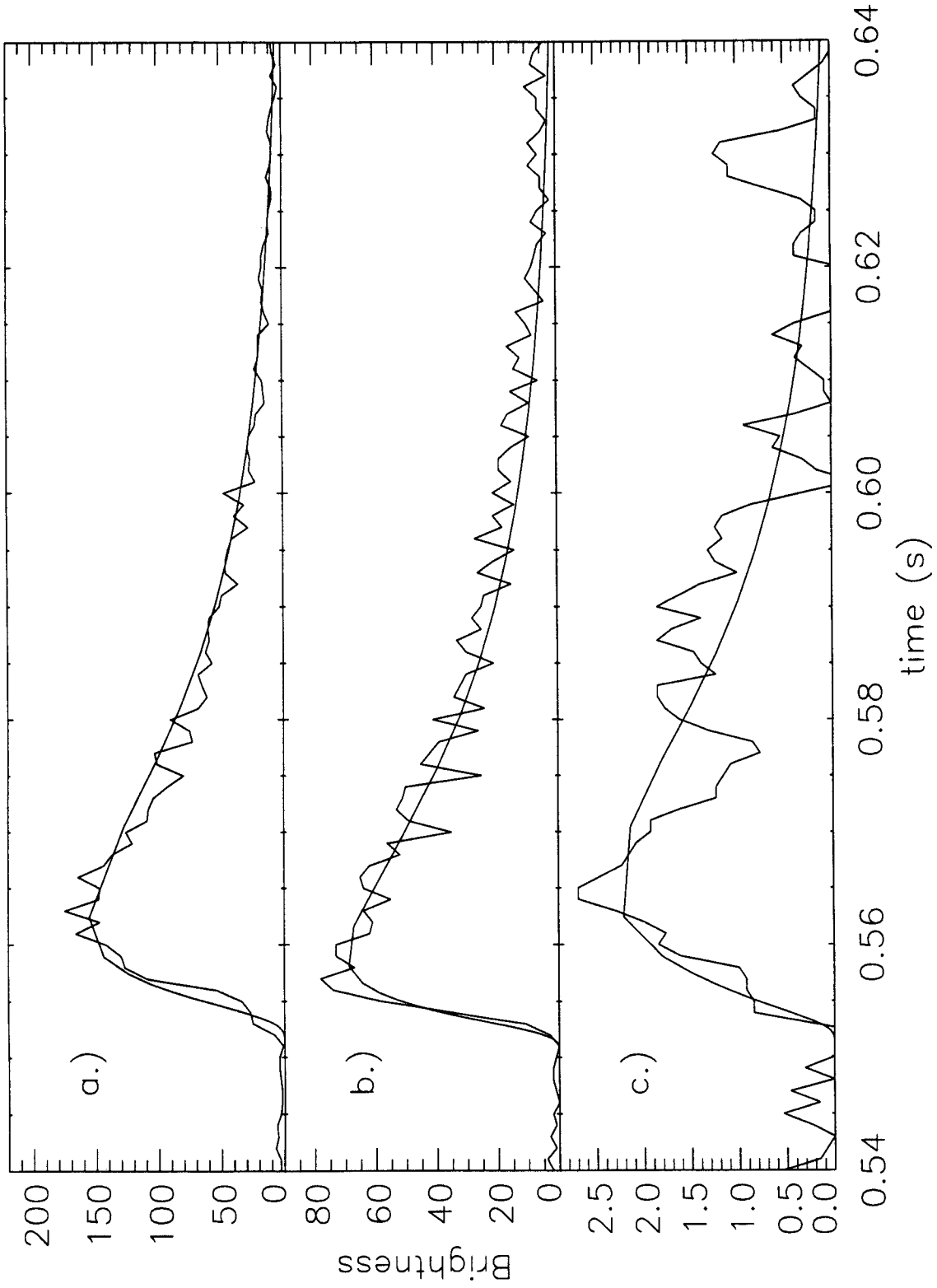
a.)
b.)
c.)
Brightness
200
150
100
50
0
80
60
40
20
0
2.5
2.0
1.5
1.0
0.5
0.0
0.54
0.56
0.58
0.60
0.62
0.64
time (s)

Figure 10

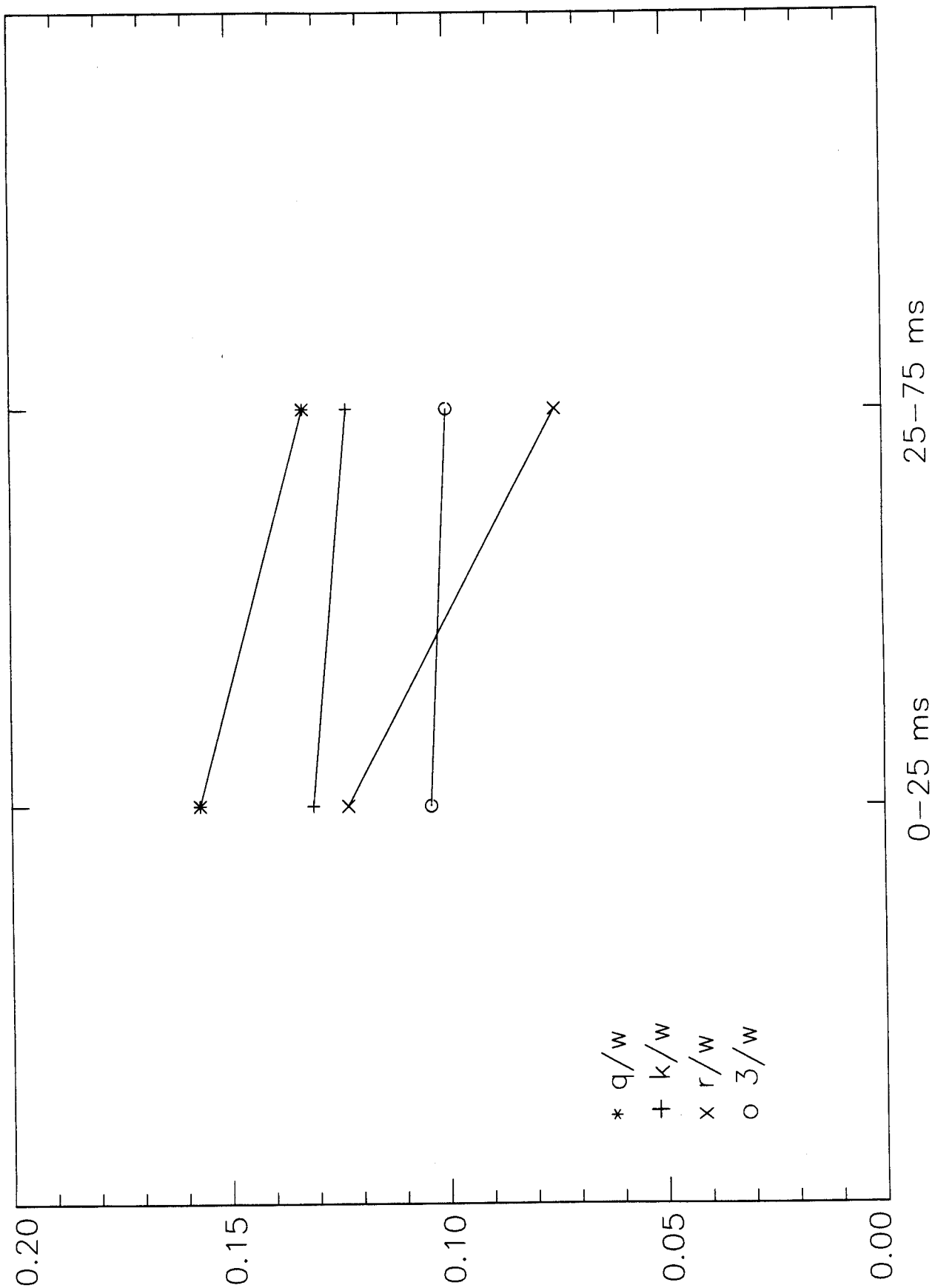

Figure 11

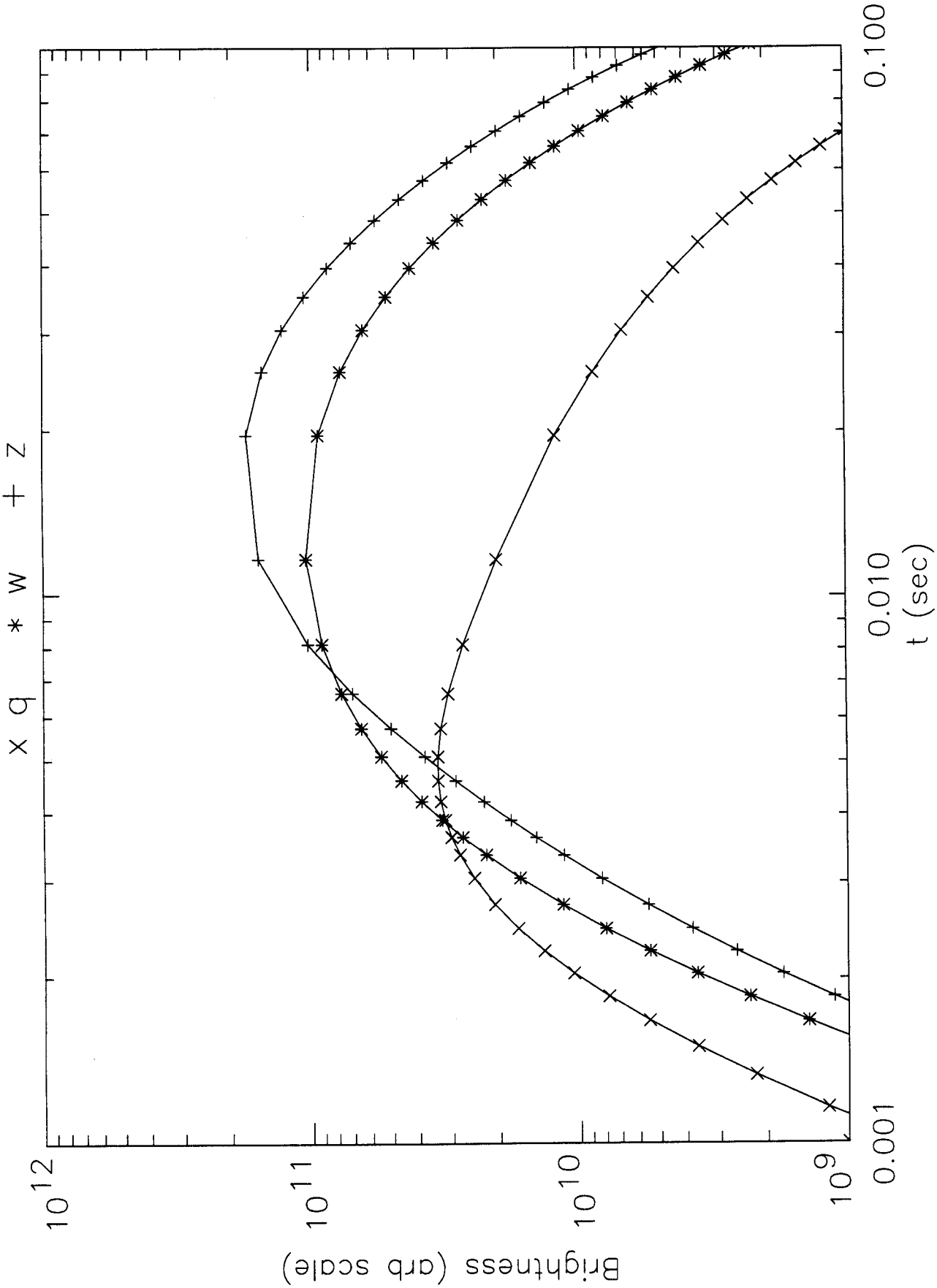
x q * w + z
Brightness (arb scale)
10^{12}
10^{11}
10^{10}
10^{9}
0.001
0.010
0.100
t (sec)

Figure 12

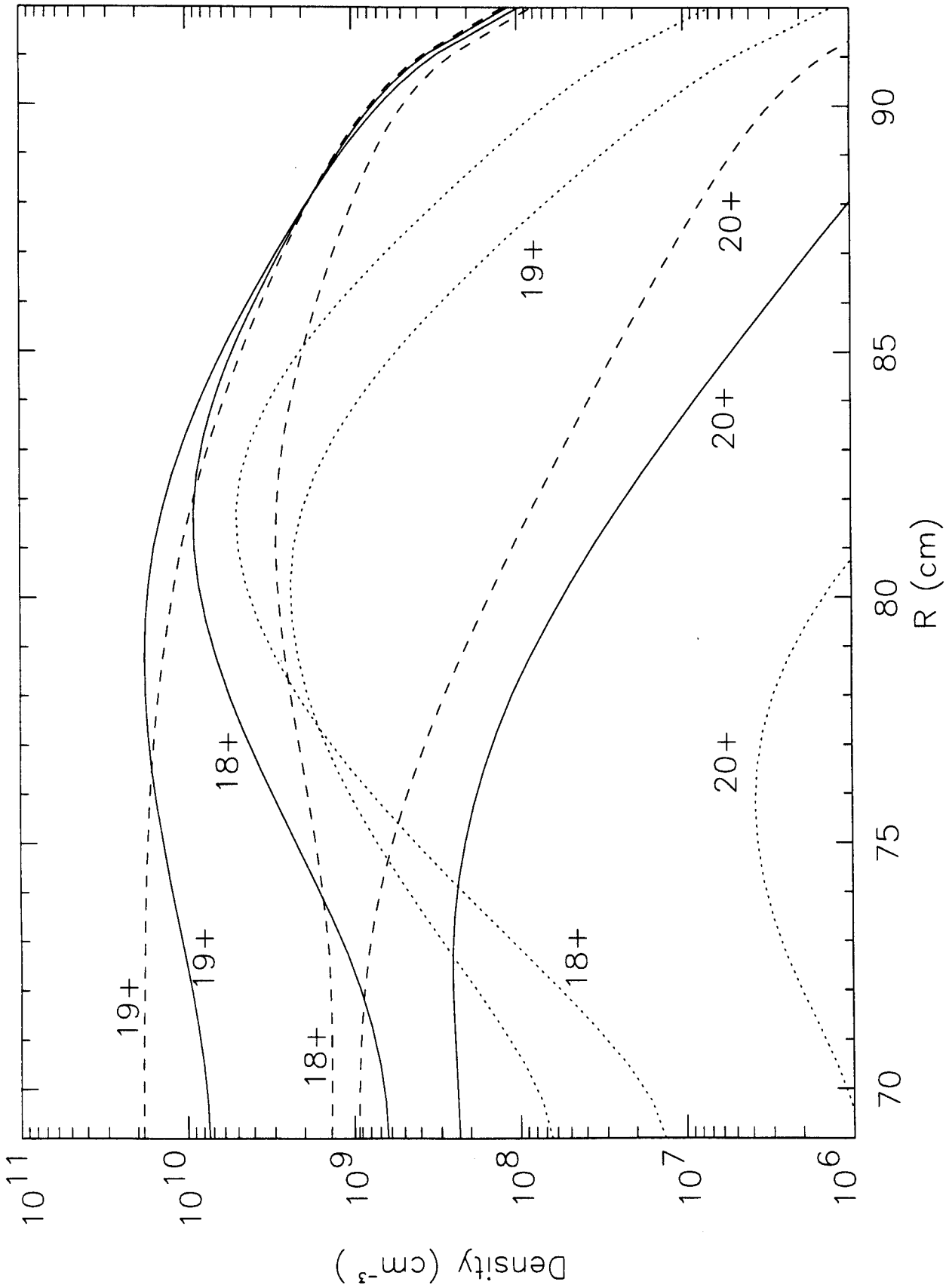
Density (cm^{-3})
10^{11}
10^{10}
10^{9}
10^{8}
10^{7}
10^{6}
70
75
80
85
90
R (cm)
19+
19+
18+
18+
19+
20+
20+
20+
18+

Figure 13

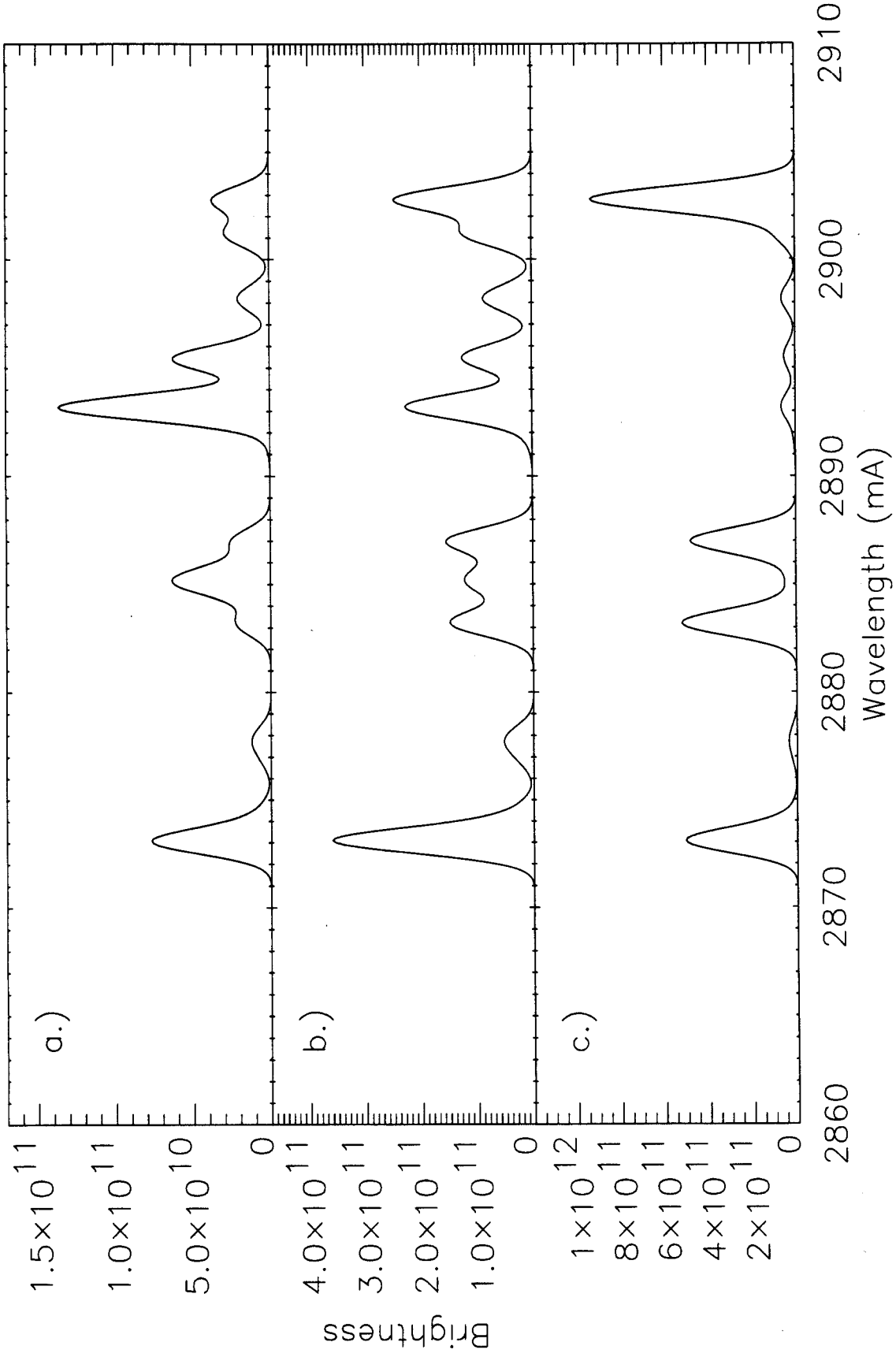
a.)
b.)
c.)
Brightness
1.5×10^11
1.0×10^11
5.0×10^10
0
4.0×10^11
3.0×10^11
2.0×10^11
1.0×10^11
0
1×10^12
8×10^11
6×10^11
4×10^11
2×10^11
0
2860
2870
2880
2890
2900
2910
Wavelength (mA)

Figure 14

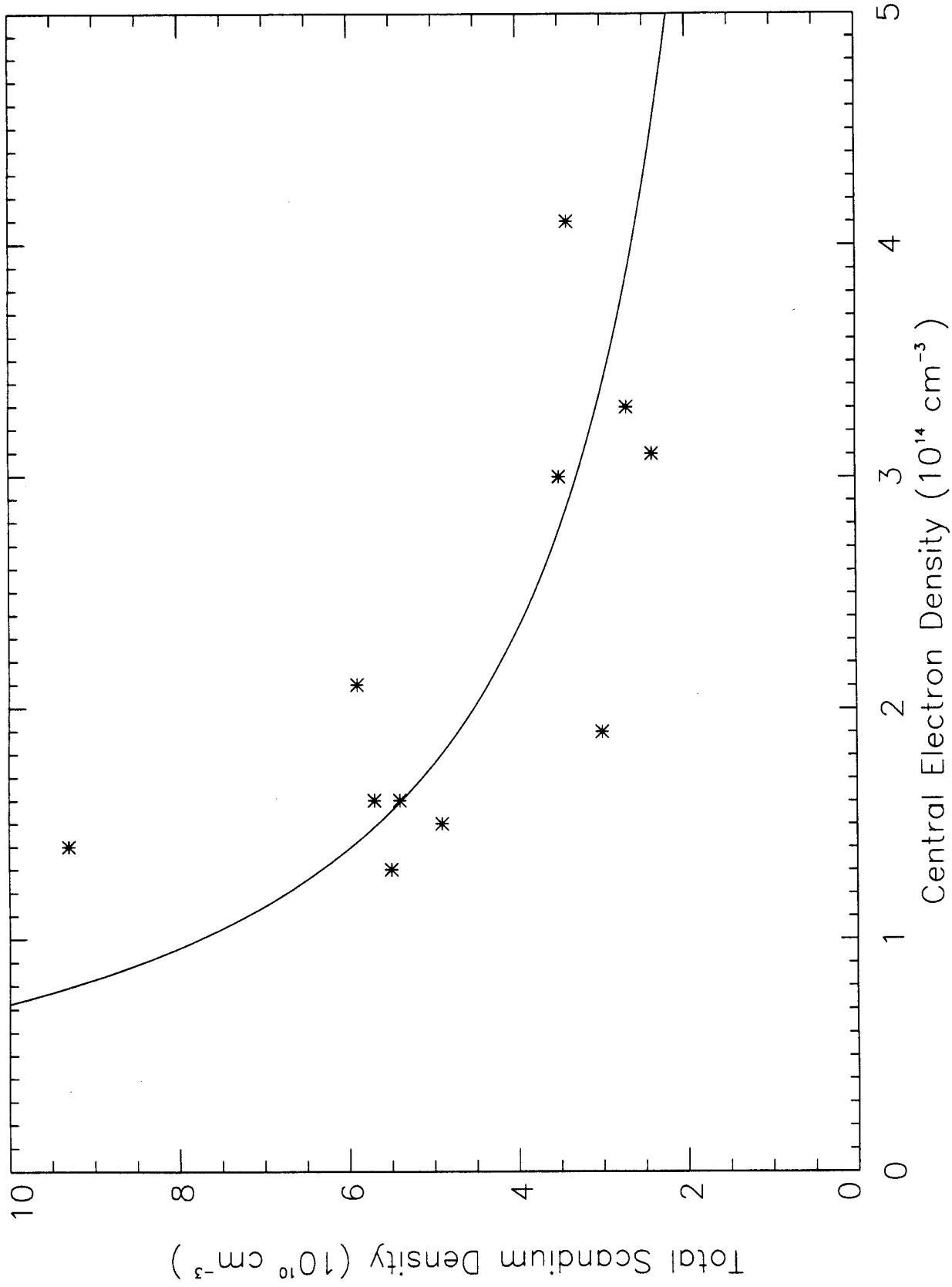
Total Scandium Density (10^{10} cm^{-3})
0
2
4
6
8
10
Central Electron Density (10^{14} cm^{-3})
0
1
2
3
4
5

Figure 15